Journal of Molecular and Cellular Cardiology 49 (2010) 132–141

Contents lists available at ScienceDirect

Journal of Molecular and Cellular Cardiology

journal homepage: www.elsevier.com/locate/yjmcc

Original article

Activation of the cardiac Na^+–Ca^{2+} exchanger by sorcin via the interaction of the respective Ca^{2+}-binding domains

Carlotta Zamparelli [a,1], Niall Macquaide [b,1], Gianni Colotti [a], Daniela Verzili [a], Tim Seidler [c], Godfrey L. Smith [b], Emilia Chiancone [a,*]

[a] C.N.R. Institute of Molecular Biology and Pathology, Department of Biochemical Sciences A. Rossi Fanelli, "Sapienza" University of Rome, 00185 Rome, Italy
[b] Institute of Biomedical and Life Sciences, University of Glasgow, Glasgow G12 8QQ, UK
[c] Department of Cardiology and Pneumology, Georg-August University, Göttingen, D-37075 Göttingen, Germany

ARTICLE INFO

Article history:
Received 1 December 2009
Received in revised form 21 January 2010
Accepted 8 March 2010
Available online 15 March 2010

Keywords:
Sorcin
Na^+/Ca^{2+} exchanger
Ca^{2+}-mediated interaction
Protein activation
Cardiomyocytes

ABSTRACT

Sorcin is a penta-EF-hand protein that interacts with intracellular target proteins after Ca^{2+} binding. The sarcolemmal Na^+/Ca^{2+} exchanger (NCX1) may be an important sorcin target in cardiac muscle. In this study, RNAi knockdown of sorcin, purified sorcin or sorcin variants was employed in parallel measurements of: (i) NCX activity in isolated rabbit cardiomyocytes using electrophysiological techniques and (ii) sorcin binding to the NCX1 calcium binding domains (CBD1 and (iii) using surface plasmon resonance and gel overlay techniques. Sorcin is activated by Ca^{2+} binding to the EF3 and EF2 regions, which are connected by the D helix. To investigate the importance of this region in the interaction with NCX1, three variants were examined: W105G and W99G, mutated respectively near EF3 and EF2, and E124A that does not bind Ca^{2+} due to a mutation at EF3. Downregulation of sorcin decreased and supplementation with wt sorcin (3 μM) increased NCX activity in isolated cardiomyocytes. The relative stimulatory effects of the sorcin variants were: W105G>wt sorcin>Sorcin Calcium Binding Domain (SCBD)>W99G>E124A. Sorcin binding to both CBD1 and 2 was observed. In the presence of 50 μM Ca^{2+}, the interaction with CBD1 followed the order W105G>SCBD>wt sorcin>W99G>E124A. In sorcin, the interacting surface can be mapped on the C-terminal Ca^{2+}-binding domain in the D helix region comprising W99. The fast association/dissociation rates that characterize the interaction of sorcin with CBD1 and 2 may permit complex formation/dissociation during an excitation/contraction cycle.

1. Introduction

Sorcin (*so*luble *r*esistance-related *c*alcium binding prote*in*) is a 21.6 kDa protein identified in the cytosol of multidrug resistant cells [1,2] that belongs to the penta-EF-hand (PEF) family, a small group of regulatory calcium binding proteins comprising calpain, ALG-2, grancalcin, peflin and PEF1 [3–8]. Sorcin shares the typical structural and functional features of all PEF family members. It has a two-domain architecture, characterized by a flexible and hydrophobic Gly/Pro-rich N-terminal domain and a C-terminal calcium binding domain containing the five EF-hand motifs (Fig. 1), and dimerizes through the unpaired EF5 hand. Like the other PEF proteins, sorcin undergoes a Ca^{2+}-dependent activation that promotes translocation to membranes where interaction with several molecular targets occurs [9]. In turn, these features render sorcin an effective participant in a number of Ca^{2+}-mediated processes. Sorcin activation is induced by Ca^{2+} binding to the two functionally relevant EF3 and EF2 motifs, that are not paired structurally as in most EF-hand proteins, but are connected by the long and rigid D helix (Fig. 1). An essential step of sorcin activation therefore consists in the transfer of information concerning Ca^{2+} binding from the site with the highest affinity for the metal, EF3, through the D helix to EF2, and from there to the rest of the molecule. The ensuing conformational change is believed to loosen the hydrophobic and hydrophilic interactions that bring the N- and C-terminal domains together. This renders both domains available for target protein recognition, in particular the D helix residues [10]. It follows that the EF3-D helix-EF2 region should be considered as a tightly coupled functional unit.

Sorcin is expressed in most human tissues including the heart where Ca^{2+}-bound sorcin interacts with and regulates several ionic channels, such as the L-type voltage-dependent channel, the ryanodine receptor, RyR2, and the sarcoplasmic reticulum Ca^{2+}-ATPase, SERCA2a, and thus plays an important role in the regulation of the excitation–contraction–relaxation processes [11–18]. Discordant effects of sorcin overexpression on cardiac function have been reported. According to Seidler et al. [13] and Meyers et al. [19] cardiac-specific overexpression of sorcin in rabbit myocytes and transgenic mice leads to a significant reduction in contractility, while

* Corresponding author. Tel.: +39 0649910761; fax: +39 064440062.
E-mail address: emilia.chiancone@uniroma1.it (C. Zamparelli).
[1] Joint first authors.

0022-2828
doi:10.1016/j.yjmcc.2010.03.003

A

N-terminal domain

MAYPGHPGAGGGYY**PGGYGGAPGGP**SFPGQTQ 1-32

C-terminal domain (SCBD)

Helix A *EF1* *Helix B* *Helix C* *EF2*
DPLYGYFASVAGQDGQIDADELQRCLTQSGIAGGYKPFNLETCRLMVSMLDRDMSGTMG 33-91

Helix D *EF3* *Helix E* *Helix F*
FNEFKELWA**V**LN**GW**RQ**H**FISFDSDRSGTVDPQELQKALTT**MGFR**LNPQTVNSIAKR 92-147

EF4 *Helix G* *EF5* *Helix H*
YSTSGKITFDDYIACCVKLRALTDSF**R**RRDSAQQ**G**MVNFSYDDFIQCVMTV 148-198

B

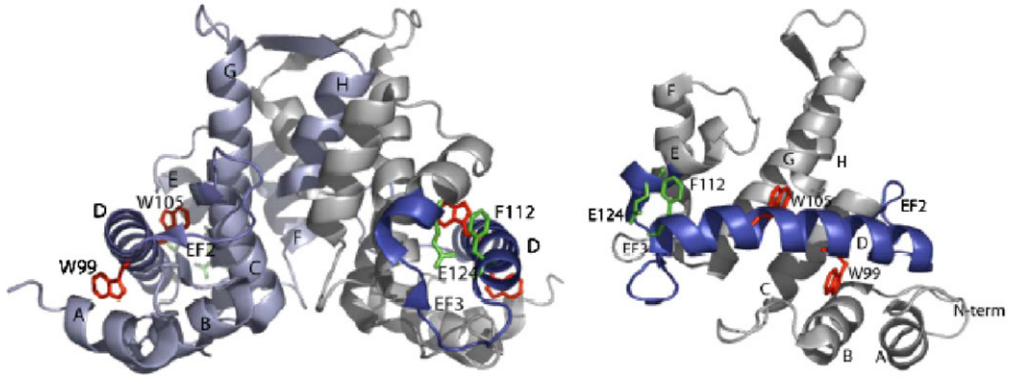

Fig. 1. Sequence of Chinese hamster sorcin and structure of the Ca^{2+}-binding domain, SCBD. (A) The amino acids of the N-terminal domain and of SCBD, involved in the interdomain contact according to Ilari et al. [10], are in boldface. The residues mutated in the variants used (W99, W105, F112 and E124) are underlined. (B) left panel. The two monomers in the SCBD dimer are depicted in different colours (light blue, gray). The D helix and the physiologically relevant EF2 and EF3 hands are coloured dark blue; the two tryptophan residues, W99 and W105, are coloured red, Phe112 and Glu124 belonging to EF3 are coloured green. (B) right panel. The gray SCBD monomer is rotated 90° with respect to the dimer presented on the left. The figure was created with PYMOL [42].

Suarez et al. [20] and Frank et al. [21] reported that transfection of rat or mouse heart or isolated cardiac cells with sorcin-expressing vectors significantly enhanced cardiac function.

The overexpression of sorcin in cardiomyocytes has also been associated with increased activity of the Na^+–Ca^{2+} exchanger, NCX [13,22]. The mammalian NCX family includes three genes (*Ncx1*, *Ncx2* and *Ncx3*) with very similar functional properties. NCX1, the main isoform expressed in the heart, catalyzes the electrogenic exchange of Ca^{2+} and Na^+ across the plasma membrane in both the Ca^{2+} influx and Ca^{2+} efflux mode and is one of the crucial regulators of Ca^{2+} homeostasis within cardiomyocytes and of cardiac contractility. NCX1 consists of nine transmembrane helices with an extracellular N-terminus and a cytosolic C-terminus that is organized in four domains [23,24]. There are two adjacent homologous Ca^{2+}-binding domains, CBD1 and CBD2, arranged in an antiparallel fashion, that are connected via a regulatory catenin-like domain (CLD) to the membrane part of the exchanger (Fig. 2). A rise in cytosolic Na^+ stimulates rapidly and then inactivates the exchanger; in contrast, cytosolic Ca^{2+} activates the exchanger and relieves the Na^+-dependent inactivation [25–28]. Regulation by cytosolic Na^+ and Ca^{2+} involves sites that do not participate directly in the ion translocation process. Thus, an amphipathic sequence, the XIP region (eXchanger *I*nhibitory *P*eptide), takes part in regulation by Na^+, whereas CBD1 and CBD2 are responsible for the Ca^{2+}-dependent activation of the exchanger. Both CBD1 and CBD2 have an Ig-like fold with the Ca^{2+}-binding sites in the distal loops [24,28,29]. They contain also an unstructured loop, the FG loop, which in CBD2 is

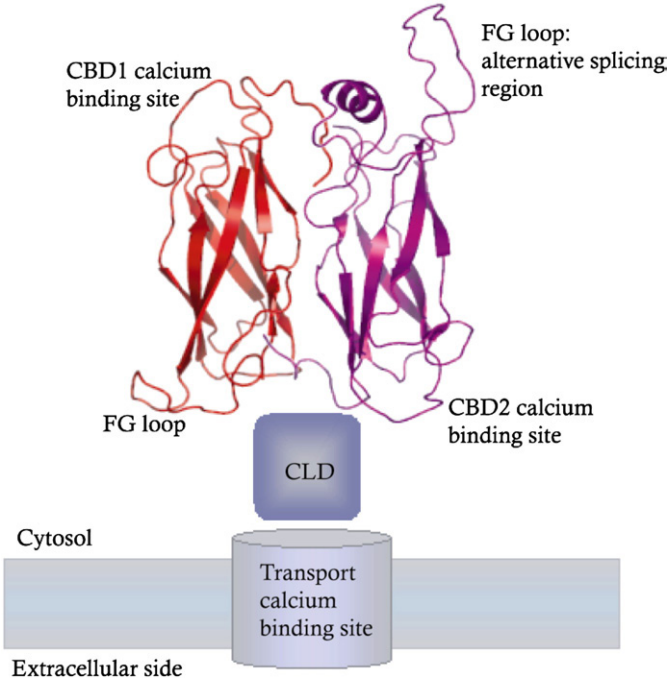

Fig. 2. Model of NCX1, according to Hilge et al. [24]. Structural details are given in the Introduction. CBD1 in red and CBD2 in magenta.

characterized by the presence of a tissue-specific, alternatively spliced region (Fig. 2). Despite the structural similarity, CBD1 binds four Ca^{2+} with high affinity ($K_D = 0.3$ μM), whereas CBD2 binds only two metal ions with lower affinity ($K_D = 5$ μM) [30]. In CBD1, the four Ca^{2+} ions are brought into close proximity by a complex arrangement of the coordinating residues. Thus, aspartate and glutamate carboxylate oxygens provide bidentate ligands that coordinate two (Asp500) or three (Glu451) Ca^{2+} simultaneously. In CBD2, the two Ca^{2+}-binding sites are only 5.4 Å apart, such that the two metal ions are coordinated by two carboxylate oxygens of a single aspartate side chain (Asp578). Mutations of acidic Ca^{2+}-binding amino acid residues in CBD1 decrease affinity for Ca^{2+}, as expected, but do not eliminate Ca^{2+}-dependent regulation [26]. In contrast, mutations E516L, D578V and E648L in the CBD2 Ca^{2+}-binding sites completely remove Ca^{2+} regulation, placing the exchanger in a constitutionally active state [28]. In accord with these observations, the alternatively spliced NCX1 kidney isoform with an arginine at position 578 and the brain isoform carrying a D578R mutation are not regulated by Ca^{2+} [31]. Taken together these data point to CBD1 and CBD2 as major determinants of the NCX1 functional regulation.

Several experimental data point to an effect of sorcin on NCX function in the heart, indicative of a possible direct interaction between the two proteins. In particular, NCX activity is increased in sorcin-overexpressing cardiomyocytes, while a low NCX activity has been observed in a rabbit model of left ventricular dysfunction (LVD) with a reduced sorcin expression level [13,22].

In the present work, the study of the sorcin-NCX1 system was investigated by parallel experiments on the isolated components and on cardiomyocytes. Overlay assay and surface plasmon resonance (SPR) experiments allowed us to establish the occurrence of a direct interaction between sorcin and the two NCX1 calcium binding domains and to characterize its kinetic and equilibrium parameters, while measurements of the NCX current in cardiomyocytes as a function of voltage furnished information on the functional effect of the interaction. Further, the surface of the sorcin molecule involved in complex formation was determined by means of previously characterized sorcin variants carrying mutations at sites involved in Ca^{2+} binding or information transfer. The effects of the mutations on the interaction parameters were assessed in surface plasmon resonance experiments, while those on function were determined by means of NCX current measurements. Specifically, the C-terminal, sorcin Ca^{2+}-binding domain (SCBD) was employed to establish whether this domain is the interacting one [4,32]; the E124A mutant was used to gain information on the Ca^{2+}-dependence of the interaction since this variant is unable to bind Ca^{2+} at physiological concentrations due to substitution of the bidentate Ca^{2+} ligand at the EF3 hand [33]; the W99G and W105G variants were utilized as selective probes of the local structural perturbations introduced by substitution of the two tryptophan residues located at the beginning and end of the D helix [34].

The results obtained point to the Ca^{2+}-dependent interaction between sorcin and NCX1 as the basis for the activation of the transporter. In sorcin, the interacting surface can be mapped on the Ca^{2+}-binding C-terminal domain in the region of the D helix comprising W99. In NCX1, both CBD1 and CBD2 participate in complex formation. Intriguingly, the rates of complex formation/dissociation are fast and could permit a beat-to-beat interaction.

2. Materials and methods

2.1. Cloning, expression and purification of sorcin and of sorcin mutants

Wild type human and Chinese hamster sorcin, SCBD (Sorcin Calcium Binding Domain) and sorcin mutants were cloned, expressed and purified as described previously [10,33,35].

2.2. Cloning, expression and purification of CBD1 and CBD2

The cDNA of *Mus musculus* NCX1 (cDNA clone MGC:90693 IMAGE:30532156) was used as template in PCR experiments in order to clone the nucleotide regions 1192–1619, encoding for CBD1 (Calcium Binding Domain 1), corresponding to amino acids 397–539, and 1581–2137, encoding for CBD2 (Calcium Binding Domain 2), corresponding to amino acids 527–712. The PCR products, digested with NdeI and HindIII restriction enzymes, were cloned in the pET22 vector. The recombinant vectors were used to transform competent *E. coli* BL21(DE3) cells. Protein expression was induced by 1 mM IPTG for 5 h at 37 °C. After sonication (1 min at 14 Hz/mL cell solution), the lysates were centrifuged at 15,000 rpm for 20 min: CBD1 was recovered in the supernatant, whereas CBD2 remained in the insoluble fraction. CBD1 purification was carried out by 30% (w/v) ammonium sulphate precipitation at room temperature for 1 h, while CBD2 purification required protein extraction by treatment with 0.3% N-lauryl-sarcosine in 50 mM CAPS buffer pH 11.0. An anion exchanger column Mono-Q (GE Healthcare) was used to improve purification of both NCX1 domains. The proteins, dialysed vs. a 10 mM Tris–HCl buffer at pH 7.5, were loaded onto the column and were recovered upon application of a linear gradient of NaCl between 0 and 0.5 M. Based on SDS page electrophoresis, the degree of enrichment was ~80% for CBD1 and ~70% for CBD2. In the SPR experiments the concentration of CBD1 and CBD2 was calculated from the intensity of the respective bands in SDS gels (Supplementary Fig. S1) after determination of the total protein concentration with the Bradford assay.

2.3. Overlay assay experiments

Wt sorcin and SCBD were subjected to electrophoresis on a 15% polyacrylamide gel under denaturing conditions [36] and transferred to polyvinyl difluoride membranes (PVDF) in transfer buffer [25 mM Tris–HCl, 192 mM glycine, and 20% methanol (pH 8.3)] at 100 mA for 45 min. The PVDF membranes were incubated at room temperature separately with CBD1 and CBD2 (20 μg/mL) in 1% gelatin in TBST buffer [20 mM Tris–HCl, 0.5 M NaCl, and 0.05% Tween 20 (pH 7.5)] containing either 50 μM $CaCl_2$ (total concentration) or 1 mM EGTA to assess the calcium dependence of the interaction. Subsequently, the membranes were incubated in 1% gelatin in TBST buffer with a mouse anti-NCX1 monoclonal antibody (antigen: purified canine cardiac NCX; Biocompare). The antibody was used at 1:3000 dilution, a condition where it recognizes equally well CBD1 and CBD2 and does not recognize other proteins like albumin and gelatin, as established in preliminary experiments. The blots were developed by incubation for 45 min with alkaline phosphatase conjugated monoclonal anti-mouse IgG in 1% gelatin in TBST. Control experiments ruled out the existence of cross reactivity between sorcin or SCBD and the anti-NCX monoclonal antibody.

2.4. Surface plasmon resonance measurements

Surface plasmon resonance (SPR) experiments were carried out using a BIACORE X system (BIAcore AB, Uppsala, Sweden). The sensor chip (CM5, Biacore AB) was activated chemically by a 35 μL injection of a 1:1 mixture of *N*-ethyl-*N*′-(3-(dimethylaminopropyl) carbodiimide (200 mM) and *N*-hydroxysuccinimide (50 mM) at a flow rate of 5 μL/min. In one set of experiments, sorcin was immobilized on the activated sensor chip via amine coupling. The reaction was carried out in 20 mM sodium acetate at pH 6.0; the remaining ester groups were blocked by injecting 1 M ethanolamine hydrochloride (35 μL). This procedure ensures immobilization of sorcin principally via the N-terminus [32]. As a control, the sensor chip was treated as described above in the absence of sorcin. The interaction of immobilized sorcin with the CBD1 and CBD2 domains of NCX1 was detected through mass

concentration-dependent changes in the refractive index on the sensor chip surface expressed as resonance units (RU). The increase in RU relative to baseline indicates complex formation; the plateau region represents the steady-state phase of the interaction, whereas the decrease in RU represents dissociation of the NCX1 calcium binding domains from immobilized sorcin after injection of buffer. A response change of 1000 RU typically corresponds to a change in the protein concentration on the sensor chip of 1 ng/mm^2 [37]. The experiments were carried out at 25 °C in 10 mM HEPES (pH 7.4), 150 mM NaCl, and 0.005% surfactant P-20. The buffer was treated with Chelex 100 to eliminate Ca^{2+} contaminations and degassed. The concentration of CBD1 and CBD2 ranged between 500 nM and 22 μM at a constant calcium concentration.

In a second set of experiments, CBD1 was immobilized on the activated CM5 chip at pH 4.5 using the procedure described above. The interaction with wt sorcin or sorcin mutants (E124A, W99G, W105G and SCBD) at a concentration of 1 μM was measured in the presence of 20 and 50 μM Ca^{2+}. Scatchard analysis of the dependence of the SPR signal at steady state (*R*eq) on the concentration of CBD1 and CBD2 was performed to determine the equilibrium dissociation constant. *R*eq values were calculated from the sensorgrams using BIAevaluation version 3.0. The amine coupling kit, the P-20 surfactant, and the CM-5 sensor chip were purchased from BIAcore AB and all the other reagents were high-purity grade.

Negative controls for the SPR experiments were obtained by transformation of *E. coli* BL21(DE3) with pET22, induction with 1 mM IPTG for 5 h at 37 °C, and subsequent sonication and centrifugation; the supernatants were treated as for the CBD1 and CBD2 preparations, but the last purification step by anion exchanger chromatography was omitted (Supplementary Fig. S1).

2.5. Measurement of NCX currents in isolated cardiac myocytes

Procedures were undertaken in accordance with the United Kingdom Animals (Scientific Procedures) Act 1986 and conform to the Guide for the Care and Use of Laboratory Animals published by the US National Institutes of Health (NIH Publication No. 85-23, revised 1985). New Zealand White male rabbits were given an intravenous injection of 500 U heparin together with an overdose of sodium pentobarbitone (100 mg/kg) and their hearts were removed. Isolated hearts were perfused retrogradely (25 mL min^{-1}, 37 °C) with a nominally Ca^{2+}-free Krebs–Henseleit solution containing 0.6 mg mL^{-1} collagenase (type 1, Worthington Chemical Co) and 0.1 mg mL^{-1} protease (type XIV, Sigma Chemical Co) for 6–8 min. After isolation of the left ventricular free wall, the epicardial layers of the free wall were isolated from the remaining tissue by dissecting a 1–1.5 mm layer from the epicardial surface. The layers of tissue were incubated separately for 5 min in enzyme solution containing 80 μmol/L $CaCl_2$ and 4% bovine serum albumin (BSA, fraction V, Sigma). The cardiomyocyte suspensions were obtained at the end of the incubation period. Isolated cardiomyocytes were superfused with a HEPES-based Tyrode's solution at 36–37 °C in a chamber mounted on the stage of an inverted microscope. Voltage clamp was achieved a using an Axoclamp 2A amplifier (Axon Instruments, Foster City, CA, USA) in discontinuous (switch clamp) mode. Pipette resistance was 1–2 MΩ. The Tyrode's solution superfusing isolated cells contained (mmol/L): NaCl (140), KCl (4), HEPES (5), $MgCl_2$ (1), $CaCl_2$ (1.8), and glucose (11.1), pH 7.4 with NaOH. The perfusate also contained strophanthidin (0.01 mmol/L) and nifedipine (0.01 mmol/L), 4-aminopyridine (5 mmol/L, to block K^+ currents) and niflumic acid (0.1 mmol/L, to block Ca^{2+}-activated Cl^- currents. The pipette solution contained (mmol/L): CsCl (45), EGTA/CaEGTA (Cs^+ 100, EGTA 50, Ca^{2+} 25), HEPES (20), $MgCl_2$ (11, calculated free $Mg^{2+} \approx 1.2$ mmol/L), and Na_2ATP (10); pH 7.25. This pipette solution was designed to buffer $[Ca^{2+}]_i$ to ~250 nmol/L (confirmed by separate $[Ca^{2+}]$ measurements). After achieving the whole-cell configuration, a period of 5–10 min was allowed for dialysis of the pipette solution into the cell. Currents were then measured in response to a 3 s ramp from −120 mV to +80 mV from the holding potential of −80 mV. An ascending ramp was chosen since this has been shown to cause less perturbation of sub-sarcolemmal $[Ca^{2+}]$ than a descending ramp, and the resulting currents are closer to those obtained using a voltage step protocol [38]. The ramp protocol was performed at 0.1 Hz, when steady-state currents were achieved; data from 12 ramps were recorded for subsequent averaging. The protocol was repeated in the presence of 5 mmol/L Ni^{2+} to obtain the background current, and this was subtracted to obtain the current attributable to NCX (see Fig. 3(A)). Sorcin or the mutant proteins were added to the intracellular pipette solution for dialysis into the cell at a concentration of 3 μM using a protocol similar to previous work, designed to supplement endogenous intracellular sorcin by comparable amounts of exogenous protein [15,16]. Allowing sorcin to dialyse into the cell for 10 to 20 min had no additional effects (data not shown). Preliminary experiments using 1 μM sorcin had no significant effect on the NCX current (see Supplementary Fig. S5). Control measurements were made by adding identical amounts of the suspension buffer. The control and experimental data were always obtained on the same experimental day.

2.6. Preparation and testing of sorcin RNAi virus

As previously described [16], a partial rabbit sorcin sequence was amplified using primers based on the known human sorcin sequence by reverse transcription of RNA from a chinchilla bastard rabbit. Sense and antisense oligonucleotides were chosen to target the 19 nucleotide segment complementary to the rabbit sorcin mRNA sequence GCAAGAUCACCUUCGAUGA and ligated downstream of a U6 promoter into vector pSIREN-DNR (BD Biosciences Clontec, Palo Alto, USA). Six different siRNA sequences were cloned into pSIREN and verified for their effectiveness in a rabbit tumor cell line VX2. Knockdown was verified via RT-PCR. The most effective siRNA was selected to generate recombinant adenovirus. Recombination with the remaining adenoviral genome using pAdeno-X vector was carried out according to the manufacturer's instructions (BD Adeno-X Expression System, BD, Biosciences Clontech, Palo Alto, USA). Infection of adult ventricular cardiomyocytes with the AdRNAi virus (100 MOI) resulted in downregulation of native sorcin expression to 27 ± 7% of control value after 36 h of quiescent culture [16]. Example blots demonstrating of downregulation of sorcin RNA and protein are shown in the online supplement (Supplementary Fig. S5).

3. Results

3.1. Sorcin modulates NCX activity in isolated rabbit cardiomyocytes

Fig. 3(A) demonstrates the protocol used to extract the membrane current associated with NCX. Previous studies have shown that the current–voltage relationship of the Ni^{2+}-sensitive current corresponds well to the predicted relationship for NCX [39]. Specific downregulation of native sorcin protein levels to <30% of control values resulted in a significant decrease in NCX activity across the voltage range (Fig. 3(B)) to approximately 50% of the control level. This suggests that native sorcin levels tonically stimulate NCX under control levels. In separate experiments, inclusion of 3 μM wt sorcin in the pipette to supplement intracellular sorcin levels resulted in a dramatic increase in NCX activity (Fig. 3(C)).

3.2. Sorcin and NCX1 interact directly by means of the respective Ca^{2+}-binding domains: overlay assay experiments

The immunoblot experiments presented in Fig. 4 show that sorcin interacts with NCX1 by means of SCBD and that the interaction

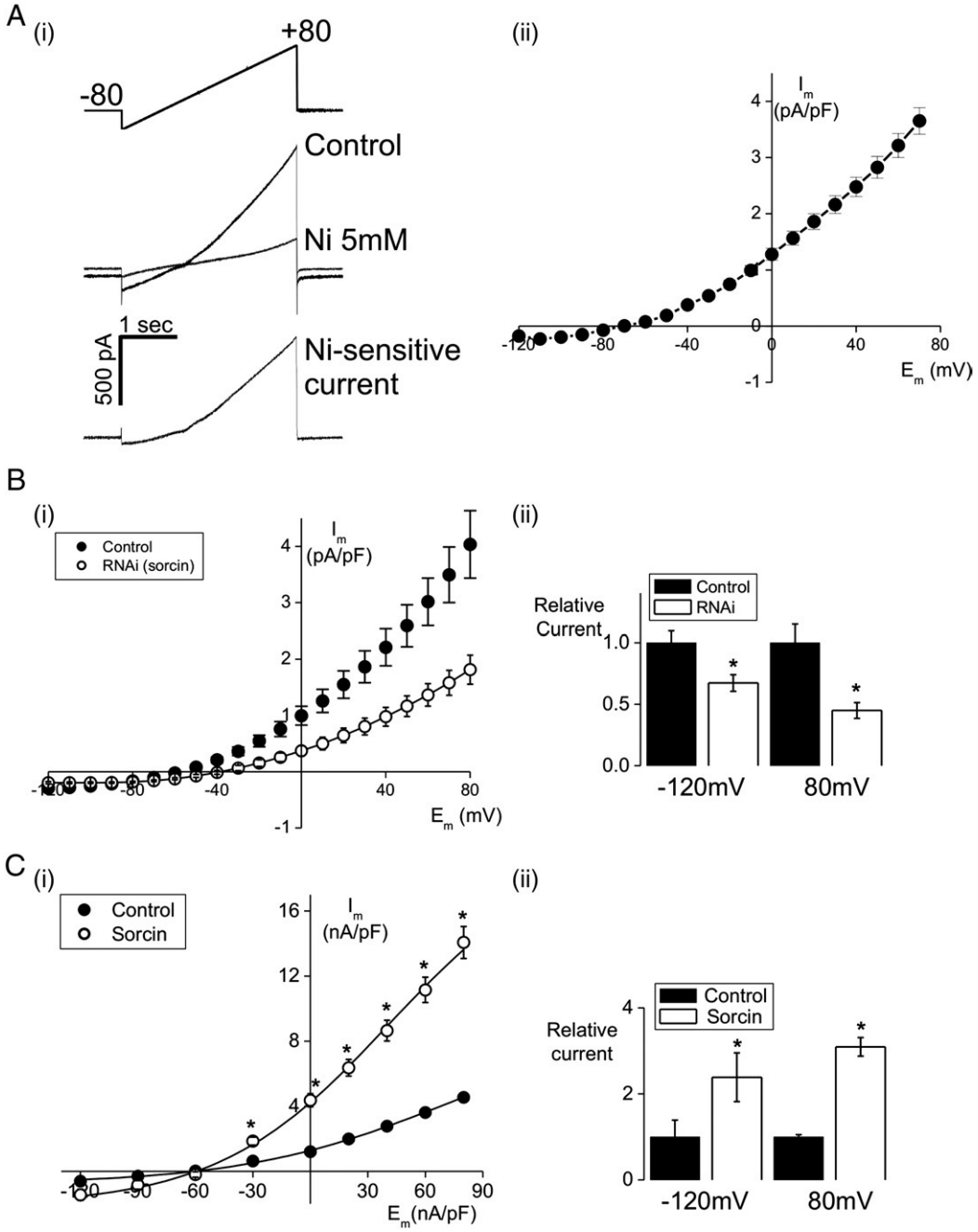

Fig. 3. Effect of sorcin and knockdown of sorcin on cardiac NCX activity. (A) The ascending voltage ramp protocol (−120 to +80 mV in 3 s) applied to a single ventricular cardiomyocyte and the associated membrane currents in the absence and presence of 5 mmol/L Ni^{2+} (the zero current level indicated by the horizontal line). The Ni^{2+}-sensitive signal (lower panel) represents the current carried by NCX (I_{NCX}). This protocol was used to generate the average I–V relationships shown in (A(ii)) for normal cardiomyocytes ($n=20$ cells from 3 hearts). (B) shows the data from cardiomyocytes transfected with mRNAi virus for sorcin compared to the Ad-LacZ control. The relative change in currents at −120 mV and +80 mV are shown in (B(ii)). I_{NCX} is lower in myocytes transfected with the mRNAi adenovirus that reduces sorcin expression. (*$P<0.05$, $n=15$ cells from 3 hearts in both groups). (C) shows the I–V curve recorded from cells with 3 μM sorcin dialysed into the cell via the intracellular pipette. I_{NCX} was significantly increased in cardiomyocytes compared to control ($n=15$ myocytes from 3 hearts in each group).

involves both CBD1 and CBD2. In the presence of 50 μM Ca^{2+}, the two NCX1 domains appear to interact with sorcin in a similar manner. When incubation is carried out in the presence of EGTA no bands are visible in the immunoblot (Supplementary Fig. S3), an indication that complex formation is specific and calcium dependent.

3.3. SPR characterization of the sorcin–NCX1 interaction

Surface plasmon resonance experiments were performed to characterize the binding reaction quantitatively. In a first series of experiments, sorcin was immobilized onto the chip. The changes in refractive index (RU) that occur during injection of the CBD1 and CBD2 solutions at different concentrations in the presence of 50 μM $CaCl_2$ are depicted in Figs. 5(A), (B) and the Scatchard analysis of the data is presented in Fig. 5(C). The equilibrium and kinetic parameters that describe the interaction of immobilized sorcin with the two NCX1 domains are rather similar. In particular, the equilibrium dissociation constant pertaining to CBD1 and CBD2 correspond to $K_D=7\pm2$ μM and 3 ± 1.7 μM, respectively. As expected, the interaction with both CBD1 and CBD2 depends on calcium concentration. At nanomolar calcium (a concentration achieved by addition of 2 mM EDTA) no interaction takes place as shown by the extremely small *R*eq values

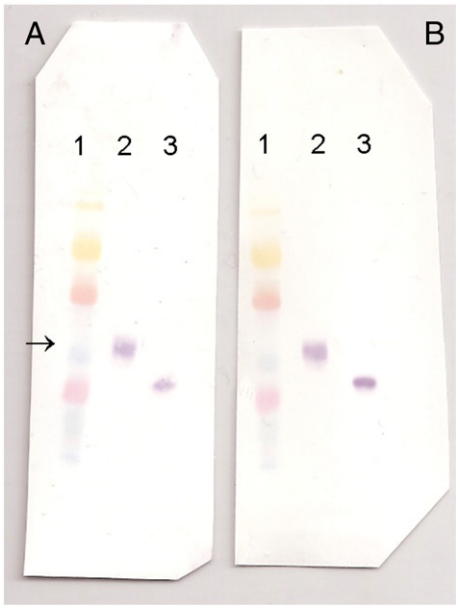

Fig. 4. Interaction of CBD1 and CBD2 with wild type sorcin and SCBD. Sorcin and SCBD (20 μg) were subjected to electrophoresis under denaturing conditions and transferred to PVDF membranes. These were incubated at room temperature with CBD1 (panel A) and CBD2 (panel B) in the presence of 50 μM $CaCl_2$ and subsequently with an anti-NCX monoclonal antibody. The blots were developed by incubation with alkaline phosphatase conjugated monoclonal anti-mouse IgG. Lane 1: molecular markers (46, 30, 21.5, and 14.3 kDa); lane 2: sorcin; lane 3: SCBD. The arrow indicates the molecular weight corresponding to sorcin.

(data not shown) while at 20 and 50 μM there is interaction and the time courses are alike. Experiments with negative control preparations ruled out the occurrence of aspecific binding (Supplementary Fig. S4).

In another set of experiments CBD1 and CBD2 were immobilized on the sensor chip and their interaction with soluble wt sorcin was measured. For CBD1, the results obtained at 50 μM Ca^{2+} yield an equilibrium constant $K_D = 1.2 \pm 2$ μM, while CBD2 interacts with sorcin with an equilibrium constant $K_D = 1.0 \pm 2$ μM, in satisfactory agreement with the data obtained with immobilized sorcin. The increase in RU at nanomolar Ca^{2+} concentration was negligible.

These observations prompted the experiment depicted in Fig. 6 aimed at mimicking the changes in Ca^{2+} concentration that occur during an excitation–contraction–relaxation cycle. Thus, wt sorcin was bound to immobilized CBD1 at 50 μM Ca^{2+} and was dissociated at nM Ca^{2+} (i.e. in the presence of 2 mM EDTA). The sorcin–CBD1 complex dissociates about ten-fold faster ($k_d = 0.9 \pm 0.4\ s^{-1}$) than at 50 μM Ca^{2+}. The parallel experiment at the latter Ca^{2+} concentration is also shown to allow a direct comparison. Similarly, wt sorcin was bound to immobilized CBD2 at 50 μM Ca^{2+} and was dissociated at nM Ca^{2+}. At this Ca^{2+} concentration the sorcin–CBD2 complex dissociates about ten-fold faster ($k_d = 0.6 \pm 0.2\ s^{-1}$) than at 50 μM Ca^{2+} just like the sorcin–CBD1 one.

The SPR results are compiled in Table 1.

3.4. Effect of sorcin mutants on NCX1 activity

The presence of 3 μM sorcin Ca^{2+}-binding domain (SCBD) increases NCX activity by about 120% relative to control suggesting this domain is important in the stimulation of NCX1 activity, in accord with its involvement in formation of the sorcin–NCX1 complex (Fig. 7). The different sorcin variants analyzed have strikingly different effects on the activity of NCX1 as already observed in the case of the Ca^{2+} spark properties which reflect RyR2 activity in cardiomyocytes [33,34]. This applies in particular to the W99G and W105G variants which carry a mutation in the D helix at a distance of only two helical turns. The W105G variant quadruplicates NCX activity with respect to control and therefore resembles wt sorcin (Fig. 3), whereas W99G increases the Ni^{2+}-sensitive currents by about 60% with respect to control. The E124A mutant, characterized by impaired binding of Ca^{2+} to the highest affinity EF3 site, is indistinguishable from control.

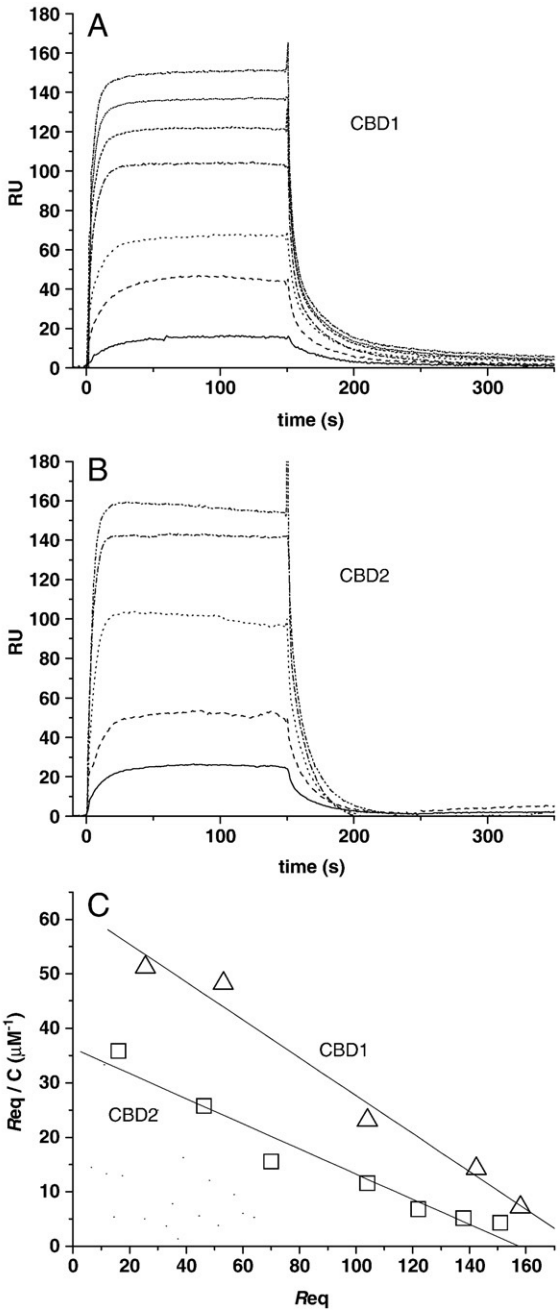

Fig. 5. SPR measurement of the interaction between immobilized wild type sorcin and the NCX1 Ca^{2+}-binding domains, CBD1 and CBD2, at different protein concentrations. The increase in RU relative to baseline indicates complex formation; the plateau region represents the steady-state phase of the interaction, whereas the decrease in RU represents dissociation of CBD1 and CBD2 from immobilized sorcin after injection of buffer. The buffer was 10 mM HEPES, 0.15 M NaCl, and 0.005% surfactant P-20 (pH 7.4), containing 50 μM $CaCl_2$. The temperature was 25 °C. The sensorgrams shown are the average of two experiments. (A) CBD1 injected at protein concentrations of 0.45, 1.8, 4.5, 9, 18, 27, and 35 μM, from bottom to top. (B) CBD2 injected at protein concentrations of 0.50, 1.1, 4.5, 10, and 22 μM, from bottom to top. (C) Scatchard plot: the plateau signal at steady state (*R*eq) measured at different CBD1 and CBD2 concentrations is plotted as a function of *R*eq/C. CBD1: Δ, CBD2: □.

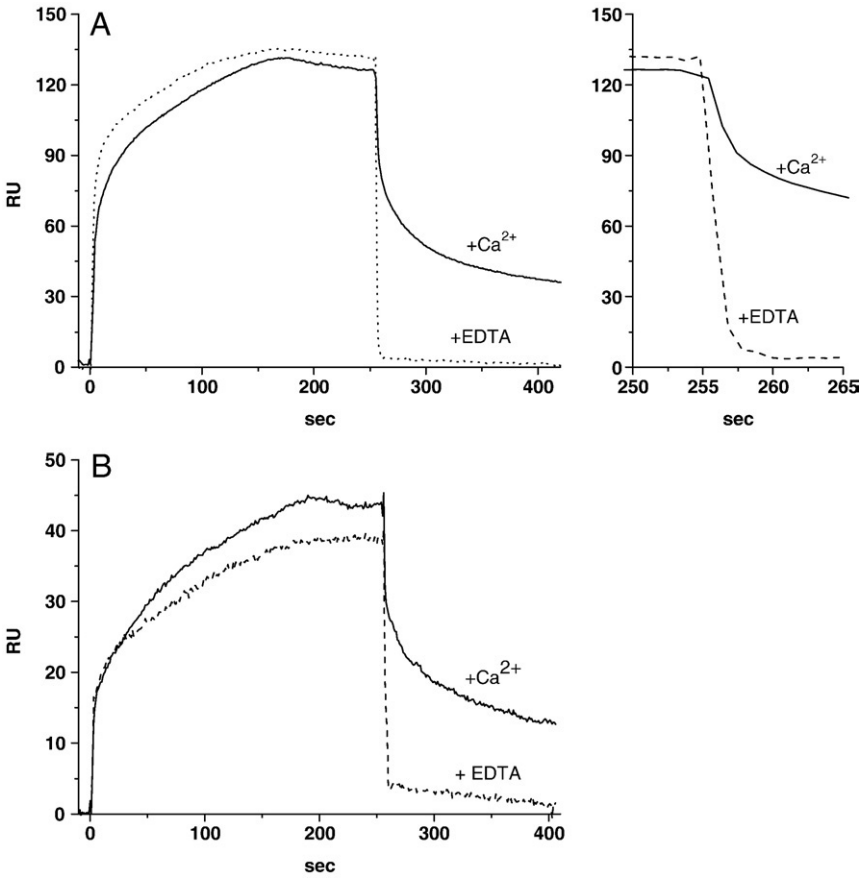

Fig. 6. SPR measurement of the interaction between wild type sorcin and immobilized CBD1 (A) and with immobilized CBD2 (B). Sorcin concentration was 6 μM in 10 mM HEPES, 0.15 M NaCl, and 0.005% surfactant P-20 (pH 7.4), containing 50 μM $CaCl_2$. The temperature was 25 °C. The increase in RU relative to baseline indicates complex formation in the presence of 50 μM $CaCl_2$, whereas the decrease in RU represents dissociation of sorcin from CBD1 after injection of buffer containing 50 μM $CaCl_2$ (solid line) or 2 mM EDTA (dashed line). The panel on the right shows the beginning of the dissociation phase. The sensorgrams are the average of two experiments.

3.5. SPR characterization of the sorcin mutants–NCX1 interaction

The NCX activity data just presented were supplemented by SPR experiments in which the interaction between immobilized CBD1 and soluble wt sorcin or sorcin variants at the same protein concentration was monitored (Fig. 8). In the presence of 50 μM Ca^{2+}, the interaction with CBD1 follows the order W105G>SCBD>wt sorcin>W99G based on the observed increase in RU. The corresponding K_D values decrease from 26 to 2.0 μM (average of two experiments). In case of the E124A variant the increase in RU was negligible.

4. Discussion

The current study demonstrates a tonic influence of sorcin on NCX; downregulation of sorcin levels decreases NCX activity and addition of wt sorcin stimulates NCX. The study also provides evidence for a direct interaction between sorcin and NCX1 and thus furnishes a molecular explanation for the activation of the exchanger associated with increased expression of sorcin in cardiomyocytes [13,22].

A dual experimental approach was used to advantage. Overlay and SPR measurements on the isolated proteins/domains allowed the kinetic and equilibrium characterization of the interaction with NCX1 subfragments while NCX activity measurements on cardiomyocytes were used to extend the conclusions thus drawn to a cellular context. In the case of sorcin, the behaviour of the wild type protein was compared to that of the Ca^{2+}-binding domain, SCBD, and of the site-specific mutants used successfully to map the surface interacting with RyR2 [34]. As far as NCX1 is concerned, the two major cytoplasmic Ca^{2+}-binding domains, CBD1 and CBD2, were chosen in view of their important regulatory role. The choice of these NCX1 domains proved to be correct based on the agreement of the NCX activity results and those of the overlay experiments (Figs. 3 and 4). Thus, sorcin increases NCX

Table 1
Equilibrium and kinetic constants for the sorcin–NCX domains interaction as assessed from SPR experiments.

	K_D (M)	k_a (M^{-1} s^{-1})	k_d (s^{-1})	k_d (s^{-1})
	50 μM $CaCl_2$	50 μM $CaCl_2$	50 μM $CaCl_2$	2 mM EDTA
Immobilized-soluble protein				
Sorcin–CBD1	$7\times10^{-6}\pm2\times10^{-6}$	$4\times10^{4}\pm1\times10^{4}$	0.27 ± 0.1	
Sorcin–CBD2	$3\times10^{-6}\pm1.7\times10^{-6}$	$8\times10^{4}\pm3\times10^{4}$	0.24 ± 0.1	
CBD1–sorcin	$1.2\times10^{-6}\pm2\times10^{-6}$	$7\times10^{4}\pm4\times10^{4}$	0.08 ± 0.1	0.9 ± 0.4
CBD2–sorcin	$1.0\times10^{-6}\pm2\times10^{-6}$	$5\times10^{4}\pm4\times10^{4}$	0.05 ± 0.03	0.6 ± 0.2

Conditions: 10 mM HEPES (pH 7.4), 150 mM NaCl, and 0.005% surfactant P-20, in the presence of 50 μM $CaCl_2$. Temperature 25 °C.

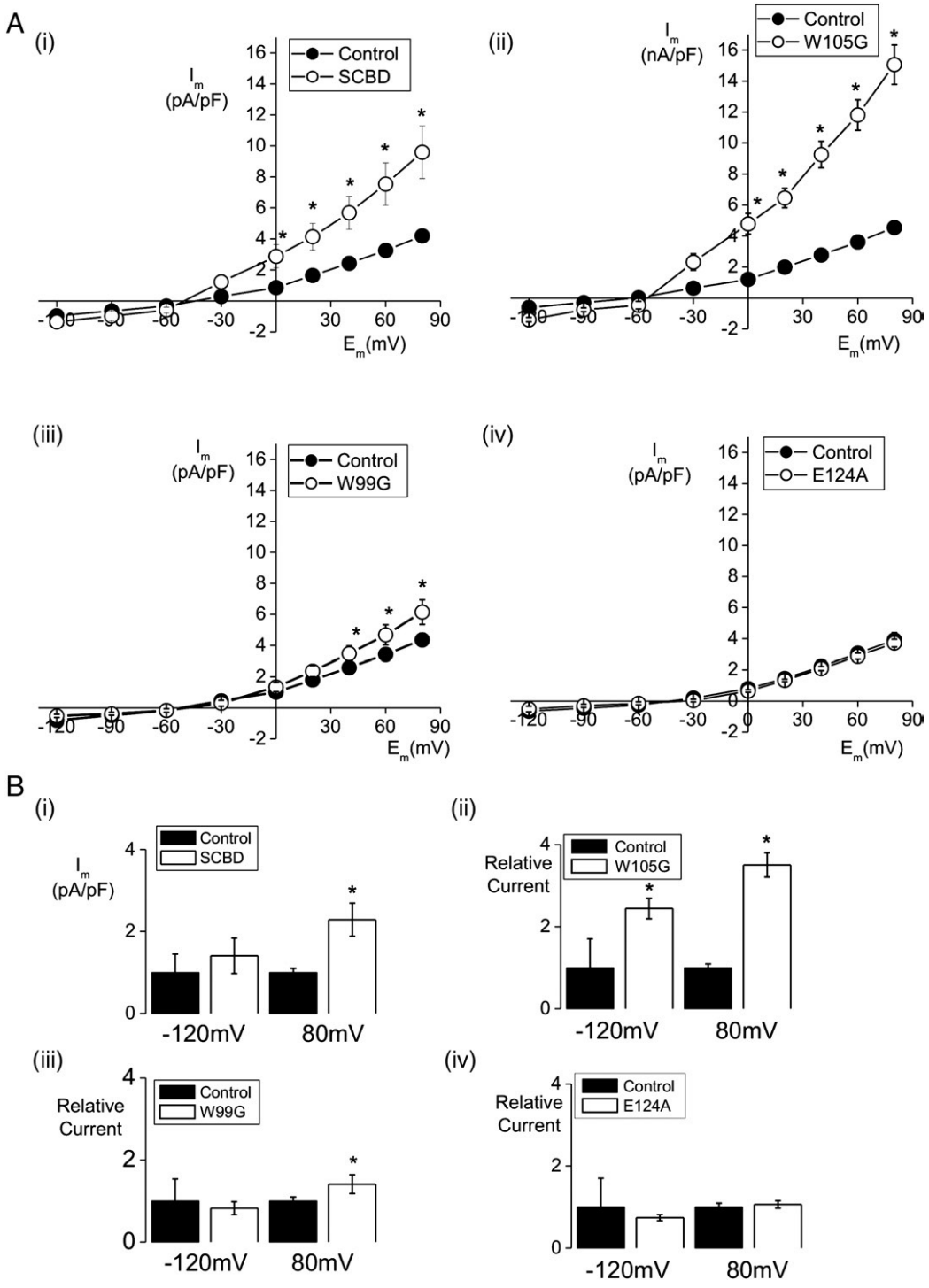

Fig. 7. Effect of sorcin variants on NCX activity. (A) shows the average Ni^{2+}-sensitive current recorded from single cardiomyocytes with a series of sorcin variants dialysed into the cell via the intracellular pipette: (i) SCBD; (ii) W105G (iii) W99G and (iv) E124A. (B) shows the relative change in I_{NCX} current at −120 and 80 mV. The variants have the following relative potency: W105G>SCBD>W99G>E124A.

activity in accordance with the observation that both CBD1 and CBD2 interact with sorcin. Both types of data also show that sorcin interacts with NCX1 via the C-terminal Ca^{2+}-binding domain. The fact that SCBD is indistinguishable from full-length sorcin in the overlay experiments, but has a somewhat lower activating effect on the Ni^{2+}-sensitive current in cardiomyocytes in turn indicates that the N-terminal sorcin domain may participate in the interaction.

The SPR analysis of the sorcin interaction with CBD1 and CBD2 confirms the involvement of both exchanger domains in complex formation and shows that the respective equilibrium and kinetic parameters are very similar. Thus, at a Ca^{2+} concentration of 50 μM, the equilibrium dissociation constant between immobilized sorcin and the two NCX1 domains is 3–7 μM resulting from an association rate constant of $4–8 \times 10^4$ M^{-1} s^{-1} and a dissociation rate constant of 0.24–0.27 s^{-1} (Fig. 5). Importantly, comparable results are obtained also in the reciprocal experiment, which entails the use of immobilized CBD1 or CBD2 (Figs. 6 and 8), an indication that steric effects due to immobilization have only a minor effect on the interaction. From a cellular perspective more informative values are obtained when association between CBD1 and sorcin takes place at 50 μM Ca^{2+} and

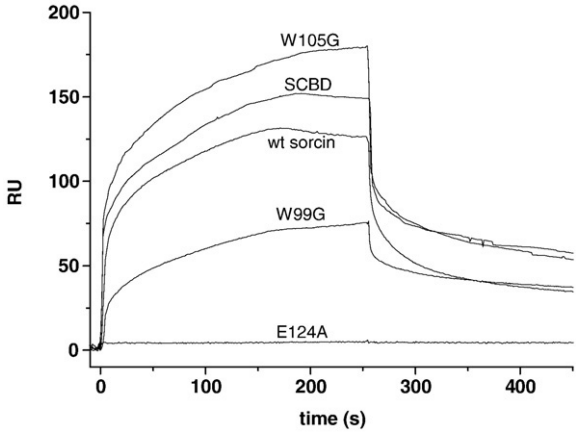

Fig. 8. Binding of wild type sorcin and sorcin variants to immobilized CBD1. Concentration of wt sorcin and variants was 6 μM, in 10 mM HEPES, 0.15 M NaCl, 50 μM $CaCl_2$, and 0.005% surfactant P-20, at pH 7.4. The increase in RU relative to baseline indicates complex formation, whereas the decrease in RU represents dissociation of sorcin from the immobilized CBD1 domain after injection of buffer. The temperature was 25 °C. The sensorgrams shown are the average of two experiments. From top to bottom: W105G, SCBD, wt sorcin, W99G, and E124A.

dissociation at nanomolar Ca^{2+} since these Ca^{2+} concentrations mimic those occurring during the excitation–contraction–relaxation cycle (Fig. 6). This experiment clearly shows that the decreased affinity of the two proteins at nanomolar Ca^{2+} can be attributed to the significant increase in the rate of dissociation of the complex ($k_d = 0.9 \pm 0.4\ s^{-1}$, corresponding to $t_{1/2}$ values of 0.5–1.4 s) upon decrease in Ca^{2+} concentration.

Having established that sorcin and NCX1 interact via the respective Ca^{2+}-binding domains and having characterized the interaction in thermodynamic and kinetic terms, the identification of the interacting surface on the sorcin molecule was addressed. The site-specific sorcin variants of EF3 hand and D helix residues used previously to identify the sorcin region involved in complex formation with RyR2 were employed [33,34]. These mutants revealed similarities and differences in the sorcin–RyR2 and sorcin–NCX systems which both involve the sorcin D helix. However, the complex with NCX1 is formed via the sorcin region near EF3 comprising W99. Thus, removal of W99 almost abolishes interaction with the exchanger (Fig. 8) and its activation (Fig. 7), while mutation of W105 leaves both properties unaltered with respect to wt sorcin. In contrast, the interaction with RyR2 is severely compromised when W105 is mutated, but is affected only marginally upon substitution of W99 [34].

The data just presented shed light only on part of the events that are triggered by Ca^{2+} binding to sorcin and NCX leading to an increased NCX activity. The affinity for Ca^{2+} is such that at low micromolar Ca^{2+} concentrations both proteins are saturated with Ca^{2+} [30,33] and acquire the conformation that renders them able to interact with fast kinetics via the respective Ca^{2+}-binding domains. The sorcin Ca^{2+}-binding domain participates also in the interaction with RyR2, but not in the sorcin–annexin VII interaction which takes place via the respective N-terminal regions [32–34]. In sorcin, the beginning of the D helix within the EF2-D helix-EF3 functional unit is a crucial spot for complex formation as indicated by the effect of the available site-specific variants employed. No such detailed information is available for the CBD1 and CBD2 domains, although it may be hypothesized that sorcin binding to CBD2 favours a conformation resembling that of its constitutionally active mutants [28]. If so, Ca^{2+}-binding sites such as E516, D578 and E648 of NCX1 could interact directly with sorcin; such interaction could remove Ca^{2+} regulation, placing the exchanger in a constitutionally active state [28]. The alternative splicing sequence of CBD2, which forms the unstructured FG loop and is accounted for being part of the regulation of NCX1 [24,40] is not important for sorcin binding, since sorcin binds similarly to CBD1 and the full-length CBD2 variant. The stoichiometry of the interaction is likewise not known. The location of the D helices on opposite sides of the sorcin dimer (Fig. 1) renders their concomitant interaction with CBD1 and CBD2 in the spatial relationship proposed by Hilge et al. [23,24] and depicted in Fig. 2 unlikely, despite the flexibility of the loops involved. Complex formation between two sorcin dimers and one NCX molecule cannot be excluded based on the available data.

As mentioned above, the interaction of sorcin with CBD1 and CBD2 is characterized by fast kinetics, both in terms of on and off rates. Both rates are fast enough to allow for a partial cycle of association with (and activation of) NCX and dissociation from (deactivation of) NCX within fractions of seconds and may allow NCX regulation on a "beat to beat" basis. The Ca^{2+} sensitive modulation would act in addition to the Ca^{2+} dependence associated with Ca^{2+} binding to the CBD1 and CBD2 domains. The reasons for two parallel levels of Ca^{2+} dependant regulation is unknown, but a similar principle appears to apply to the regulation of L-type Ca^{2+} channel, RyR2 and SERCA i.e. modulation by direct interaction of Ca^{2+} and indirectly via Ca^{2+}-dependent sorcin interaction. Further work is required to determine what aspect of cell function is mediated by this parallel series of Ca^{2+}-dependent interactions.

In more general terms, NCX has an important role in Ca^{2+} homeostasis in a variety of tissues, such as the heart, the kidney and the brain, and is a key player in pathological situations that involve dysregulation of Ca^{2+} balance [41]. The calcium-dependent translocation of sorcin to membranes, and its ability to interact with different targets (in heart, brain and other tissues) and to alter their activity, makes sorcin an efficient regulator of different functions in different cell types. The activatory role of sorcin can be important in short-term and long-term regulation of NCX1 and may have an impact in diverse pathologies where NCX1 is involved. In heart cells, the effects of sorcin on intracellular Ca^{2+} and contractility is difficult to predict, as it will depend on the status of the target channels (L-type Ca^{2+} channel and ryanodine receptor), pumps (sarcoplasmic reticulum Ca-ATPase) and exchangers (NCX1). For instance the discrepancy between sorcin-mediated decrease in intracellular Ca^{2+} reported in rabbit myocytes [13] and sorcin-mediated decrease in intracellular Ca^{2+} reported in rat myocardium [20,21] may be explained by the higher intracellular Na^+ in rat heart. Under these conditions, the capacity for Ca^{2+} extrusion is reduced and consequently the ability of sorcin to stimulate Ca^{2+} efflux is limited. Therefore additional effects on L-type, RyR or SR Ca^{2+}-ATPase may dominate and promote contractility. Alternatively in rabbit, the low intracellular Na^+ will ensure that NCX extrudes Ca^{2+} during diastole; therefore, sorcin-mediated stimulation of NCX will lower intracellular Ca^{2+} and this effect may dominate over the others in determining intracellular Ca^{2+} signals.

Acknowledgments

MIUR local funds to E.C. and MIUR PRIN 2007 grant to G.C. are acknowledged. A grant from the British Heart Foundation (No PG/04/058) to G.L.S. supported this work. TS was supported by a grant from the Deutsche Forschungsgemeinschaft (DFG) Grant Ha 1233/7-3).

Appendix A. Supplementary data

Supplementary data associated with this article can be found, in the online version, at doi:10.1016/j.yjmcc.2010.03.003.

References

[1] Meyers MB, Biedler JL. Increased synthesis of a low molecular weight protein in vincristine-resistant cells. Biochem Biophys Res Commun 1981;99:228–35.

[2] Van der Bliek AM, Meyers MB, Biedler JL, Hes E, Borst P. A 22-kd protein (sorcin/V19) encoded by an amplified gene in multidrug-resistant cells, is homologous to the calcium-binding light chain of calpain. EMBO J 1986;5:3201–8.
[3] Blanchard H, Grochulski P, Li Y, Arthur JS, Davies PL, Elce JS, et al. Structure of a calpain Ca(2+)-binding domain reveals a novel EF-hand and Ca(2+)-induced conformational changes. Nat Struct Biol 1997;4:532–8.
[4] Zamparelli C, Ilari A, Verzili D, Giangiacomo L, Colotti G, Pascarella S, et al. Structure–function relationships in sorcin, a member of the penta EF-hand family. Interaction of sorcin fragments with the ryanodine receptor and an *Escherichia coli* model system. Biochemistry 2000;39:658–66.
[5] Vito P, Lacana E, D'Adamio L. Interfering with apoptosis: Ca(2+)-binding protein ALG-2 and Alzheimer's disease gene ALG-3. Science 1996;271:521–5.
[6] Lollike K, Johnsen AH, Durussel I, Borregaard N, Cox JA. Biochemical characterization of the penta-EF-hand protein grancalcin and identification of L-plastin as a binding partner. J Biol Chem 2001;276:17762–9.
[7] Kitaura Y, Watanabe M, Satoh H, Kawai T, Hitomi K, Maki M. Peflin, a novel member of the five-EF-hand-protein family, is similar to the apoptosis-linked gene 2 (ALG-2) protein but possesses nonapeptide repeats in the N-terminal hydrophobic region. Biochem Biophys Res Commun 1999;263:68–75.
[8] Vernarecci S, Colotti G, Ornaghi P, Schiebel E, Chiancone E, Filetici P. The yeast penta-EF protein Pef1p is involved in cation-dependent budding and cell polarization. Mol Microbiol 2007;65:1122–38.
[9] Meyers MB, Zamparelli C, Verzili D, Dicker AP, Blanck TJ, Chiancone E. Calcium-dependent translocation of sorcin to membranes: functional relevance in contractile tissue. FEBS Lett 1995;357:230–4.
[10] Ilari A, Johnson KA, Nastopoulos V, Verzili D, Zamparelli C, Colotti G, et al. The crystal structure of the sorcin calcium binding domain provides a model of Ca^{2+}-dependent processes in the full-length protein. J Mol Biol 2002;317:447–58.
[11] Matsumoto T, Hisamatsu Y, Ohkusa T, Inoue N, Sato T, Suzuki S, et al. Sorcin interacts with sarcoplasmic reticulum Ca(2+)-ATPase and modulates excitation–contraction coupling in the heart. Basic Res Cardiol 2005;100:250–62.
[12] Rueda A, Song M, Toro L, Stefani E, Valdivia HH. Sorcin modulation of Ca^{2+} sparks in rat vascular smooth muscle cells. J Physiol 2006;576:887–901.
[13] Seidler T, Miller SL, Loughrey CM, Kania A, Burow A, Kettlewell S, et al. Effects of adenovirus-mediated sorcin overexpression on excitation–contraction coupling in isolated rabbit cardiomyocytes. Circ Res 2003;93:132–9.
[14] Lokuta AJ, Meyers MB, Sander PR, Fishman GI, Valdivia HH. Modulation of cardiac ryanodine receptors by sorcin. J Biol Chem 1997;272:25333–8.
[15] Farrell EF, Antaramian A, Rueda A, Gomez AM, Valdivia HH. Sorcin inhibits calcium release and modulates excitation–contraction coupling in the heart. J Biol Chem 2003;278:34660–6.
[16] Fowler MR, Colotti G, Chiancone E, Higuchi Y, Seidler T, Smith GL. Complex modulation of L-type Ca(2+) current inactivation by sorcin in isolated rabbit cardiomyocytes. Pflugers Arch 2009;457:1049–60.
[17] Fowler MR, Colotti G, Chiancone E, Smith GL, Fearon IM. Sorcin modulates cardiac L-type Ca^{2+} current by functional interaction with the alpha1C subunit in rabbits. Exp Physiol 2008;93:1233–8.
[18] Meyers MB, Puri TS, Chien AJ, Gao T, Hsu PH, Hosey MM, et al. Sorcin associates with the pore-forming subunit of voltage-dependent L-type Ca^{2+} channels. J Biol Chem 1998;273:18930–5.
[19] Meyers MB, Fischer A, Sun YJ, Lopes CM, Rohacs T, Nakamura TY, et al. Sorcin regulates excitation–contraction coupling in the heart. J Biol Chem 2003;278:28865–71.
[20] Suarez J, Belke DD, Gloss B, Dieterle T, McDonough PM, Kim YK, et al. In vivo adenoviral transfer of sorcin reverses cardiac contractile abnormalities of diabetic cardiomyopathy. Am J Physiol Heart Circ Physiol 2004;286:H68–75.
[21] Frank KF, Bolck B, Ding Z, Krause D, Hattebuhr N, Malik A, et al. Overexpression of sorcin enhances cardiac contractility in vivo and in vitro. J Mol Cell Cardiol 2005;38:607–15.
[22] Smith GL, Elliott EE, Kettlewell S, Currie S, Quinn FR. Na(+)/Ca(2+) exchanger expression and function in a rabbit model of myocardial infarction. J Cardiovasc Electrophysiol 2006;17(Suppl 1):S57–63.
[23] Hilge M, Aelen J, Perrakis A, Vuister GW. Structural basis for Ca^{2+} regulation in the Na^{+}/Ca^{2+} exchanger. Ann N Y Acad Sci 2007;1099:7–15.
[24] Hilge M, Aelen J, Vuister GW. Ca2+ regulation in the Na^{+}/Ca^{2+} exchanger involves two markedly different Ca^{2+} sensors. Mol Cell 2006;22:15–25.
[25] Hilgemann DW, Matsuoka S, Nagel GA, Collins A. Steady-state and dynamic properties of cardiac sodium–calcium exchange. Sodium-dependent inactivation. J Gen Physiol 1992;100:905–32.
[26] Matsuoka S, Nicoll DA, Hryshko LV, Levitsky DO, Weiss JN, Philipson KD. Regulation of the cardiac Na^{+}–Ca^{2+} exchanger by Ca^{2+}. Mutational analysis of the Ca^{2+}-binding domain. J Gen Physiol 1995;105:403–20.
[27] DiPolo R, Beauge L. Sodium/calcium exchanger: influence of metabolic regulation on ion carrier interactions. Physiol Rev 2006;86:155–203.
[28] Besserer GM, Ottolia M, Nicoll DA, Chaptal V, Cascio D, Philipson KD, et al. The second Ca^{2+}-binding domain of the Na^{+}–Ca^{2+} exchanger is essential for regulation: crystal structures and mutational analysis. Proc Natl Acad Sci U S A 2007;104:18467–72.
[29] Nicoll DA, Sawaya MR, Kwon S, Cascio D, Philipson KD, Abramson J. The crystal structure of the primary Ca^{2+} sensor of the Na^{+}/Ca^{2+} exchanger reveals a novel Ca^{2+} binding motif. J Biol Chem 2006;281:21577–81.
[30] Boyman L, Mikhasenko H, Hiller R, Khananshvili D. Kinetic and equilibrium properties of regulatory calcium sensors of NCX1 protein. J Biol Chem 2009;284:6185–93.
[31] Dunn J, Elias CL, Le HD, Omelchenko A, Hryshko LV, Lytton J. The molecular determinants of ionic regulatory differences between brain and kidney Na^{+}/Ca^{2+} exchanger (NCX1) isoforms. J Biol Chem 2002;277:33957–62.
[32] Verzili D, Zamparelli C, Mattei B, Noegel AA, Chiancone E. The sorcin–annexin VII calcium-dependent interaction requires the sorcin N-terminal domain. FEBS Lett 2000;471:197–200.
[33] Mella M, Colotti G, Zamparelli C, Verzili D, Ilari A, Chiancone E. Information transfer in the penta-EF-hand protein sorcin does not operate via the canonical structural/functional pairing. A study with site-specific mutants. J Biol Chem 2003;278:24921–8.
[34] Colotti G, Zamparelli C, Verzili D, Mella M, Loughrey CM, Smith GL, et al. The W105G and W99G sorcin mutants demonstrate the role of the D helix in the Ca(2+)-dependent interaction with annexin VII and the cardiac ryanodine receptor. Biochemistry 2006;45:12519–29.
[35] Franceschini S, Ilari A, Verzili D, Zamparelli C, Antaramian A, Rueda A, et al. Molecular basis for the impaired function of the natural F112L sorcin mutant: X-ray crystal structure, calcium affinity, and interaction with annexin VII and the ryanodine receptor. FASEB J 2008;22:295–306.
[36] Laemmli UK. Cleavage of structural proteins during the assembly of the head of bacteriophage T4. Nature 1970;227:680–5.
[37] Chaiken I, Rose S, Karlsson R. Analysis of macromolecular interactions using immobilized ligands. Anal Biochem 1992;201:197–210.
[38] Convery MK, Hancox JC. Comparison of Na^{+}–Ca^{2+} exchange current elicited from isolated rabbit ventricular myocytes by voltage ramp and step protocols. Pflugers Arch 1999;437:944–54.
[39] Weber CR, Ginsburg KS, Philipson KD, Shannon TR, Bers DM. Allosteric regulation of Na/Ca exchange current by cytosolic Ca in intact cardiac myocytes. J Gen Physiol 2001;117:119–31.
[40] Bano D, Young KW, Guerin CJ, Lefeuvre R, Rothwell NJ, Naldini L, et al. Cleavage of the plasma membrane Na^{+}/Ca^{2+} exchanger in excitotoxicity. Cell 2005;120:275–85.
[41] Lytton J. Na^{+}/Ca^{2+} exchangers: three mammalian gene families control Ca^{2+} transport. Biochem J 2007;406:365–82.
[42] DeLano WL. The PyMOL User's Manual. Palo Alto, CA, USA: DeLano Scientific; 2002.